Cite this: DOI: 10.1039/c0xx00000x

www.rsc.org/xxxxxx

ARTICLE TYPE

Self-Assembled Synthesis of Hierarchical Zn_2GeO_4 Core-Shell Microspheres with Enhanced Photocatalytic Activity

Weiwei Zhao, Chao Zhang, Yanmei Shi, Rui Wu, and Bin Zhang*

Received (in XXX, XXX) Xth XXXXXXXXX 20XX, Accepted Xth XXXXXXXXX 20XX
DOI: 10.1039/b000000x

Hierarchically spherical materials with core-shell structure are of special interest for a variety of promising applications. Although some advanced synthetic methods have been reported, the development of a facile strategy to fabricate hierarchically spherical materials with core-shell structure is still desirable. Herein, hierarchical Zn_2GeO_4 core-shell microspheres, with stacked nanoparticles at the core and well-aligned rods at the shell, are successfully synthesized through a triethylenetetramine (TETA)-induced self-assembly route. It exhibits relatively high photocatalytic activity and stability towards degradation of organic pollutants under UV light irradiation. In addition, other diverse hierarchical Zn_2GeO_4 macrocrystals can be successfully prepared by rationally tuning the reaction parameters. The present synthetic strategy may allow access to fabricating other multifunctional materials with special artistical morphologies.

1. Introduction

Hierarchical materials have triggered considerable attention due to their intriguing applications in photocatalysis,[1-3] solar cells,[4, 5] batteries[6-8] and thermoelectrics[9, 10]. The unique hierarchical geometrical configuration endows these materials with more attractive chemical and physical properties.[11-13] Recent examples of such hierarchical materials include spindles,[14] multipods,[15] stars,[16] dendrites[17] and other abundant structures.[18-21] As a typical example, inorganic hierarchically microspherical structures, consisting of one or two-dimensional arrangement of nanoparticles, have possessed unique merits of large specific surface area, high concentration of porosity, rich active sites and large void space.[22-26] To date, these materials, including metals,[27, 28] carbides,[29, 30] oxides,[31] sulphides,[32, 33] and selenides,[34] have been fabricated via a variety of growth techniques. In particular, inorganic hierarchically spherical materials with core-shell structure have attracted special attention.[35-37] For instance, hierarchical Fe_3O_4@C and Fe@C monodispersed core-shell microspheres were synthesized through two steps of solvothermal/hydrothermal treatments and high-temperature calcinations.[35] Ag core-shell hierarchical microstructures, with nanosheet-assembled microspheres as the core and dendrites coated on the surface, have been synthesized on FTO substrates via electrochemical deposition.[36] Hierarchical core-shell porous carbons were template-synthesized from a core-shell silica sphere assembly.[37] Despite the advances in fabricating hierarchically spherical core-shell structured materials, the exploitation of a facile and efficient hard-template-free hydrothermal approach is highly desirable. Furthermore, the hierarchical core-shell microsphere with stacked nanoparticles at the core and well-aligned rods at the shell still remains untouched. Thus, it deserves our efforts to fabricate a hierarchical core-shell microsphere with stacked nanoparticles at the core and well-aligned rods at the shell through a facile and efficient hard-template-free hydrothermal approach.

Recently, germanates, as an important class of inorganic semiconductor materials, have received great attention for its extensive applications in catalysis,[38] electronics,[39] lithium ion batteries[40, 41] and luminescence[42-44]. Among them, zinc germanate (Zn_2GeO_4), with a wide bandgap of 4.68 eV, has been considered as a multifunctional photocatalyst.[45-48] It shows efficient and stable photocatalytic activity towards degradation of organic pollutant,[45, 46] splitting of water[47] and reduction of CO_2[48]. Over the past years, diverse types of Zn_2GeO_4 nanostructures, such as nanorods,[49, 50] nanowires,[51, 52] nanoribbons,[53, 54] and nanobundles,[55] have been successfully fabricated by a series of advanced methods. The three-dimensional (3D) ordered Zn_2GeO_4 superstructures based on one-dimensional (1D) Zn_2GeO_4 nanoscale building blocks are of great importance as those architectures may achieve enhanced properties arising from hierarchical structures.[56-58] However, to date, creating hierarchical core-shell structures of Zn_2GeO_4 are still desirable. In particular, hierarchical Zn_2GeO_4 core-shell microspheres, consisting of stacked nanoparticles at the core and well-aligned rods at the shell, have not been reported yet.

Herein, we synthesize a hierarchical Zn_2GeO_4 core-shell microspheres with stacked nanoparticles at the core and well-aligned rods at the shell through a triethylenetetramine (TETA)-induced self-assembly route under a mild solvothermal hard-template-free condition (Scheme 1). In the synthetic process, alkylamine molecules act as both molecular-template and inducing agent for the assembling behaviour. Furthermore, the hierarchical Zn_2GeO_4 core-shell microspheres possess superior catalytic performance, stability and durability towards photocatalytic degradation of organic pollutants.

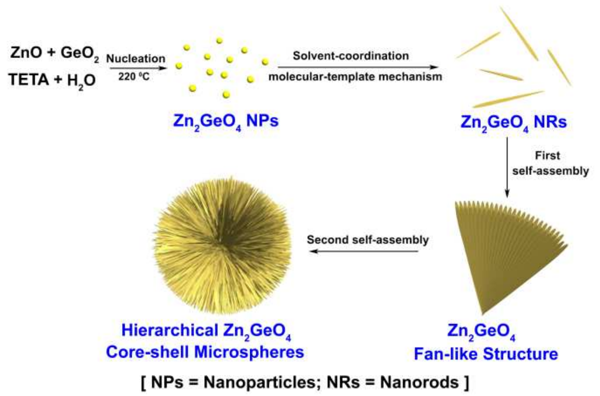

Scheme 1. Schematic illustration of the formation process of the hierarchical Zn_2GeO_4 core-shell microspheres.

2. Experience Section

2.1 Chemicals

All chemicals are analytical grade and used as received without further purification.

2.2 Synthesis of the hierarchical Zn_2GeO_4 core-shell microspheres

In a typical synthesis, 0.1046 g of GeO_2 (1.0 mmol) and 0.1628 g of ZnO (2.0 mmol) are added to 13 mL solvent including 8 mL deionezd water and 5 mL triethylenetetramine (TETA). The mixture immediately becomes milky and is stirred for 20 min at ambient conditions. Then, the solution is transferred to a 20 mL stainless Teflon-lined autoclave and maintained at 220 ^{o}C for 24 h. Afterward, the autoclave is cooled naturally to room temperature. The sample is collected by centrifugation, washed thoroughly with deionized water and alcohol several times, and then dried at 60 ^{o}C for 12 h.

2.3 Characterization

The scanning electron microscopy (SEM) images are taken with a Hitachi S-4800 scanning electron microscope (SEM, 5 kV) equipped with the Thermo Scientific energy-dispersion X-ray fluorescence analyzer. Transmission electron microscopy (TEM), high-magnification transmission electron microscopy (HRTEM) and Energy-dispersive X-ray spectroscopic (EDS) analysis are performed with JEOL-2100F system equipped with EDAX Genesis XM2. Specimens for TEM and HRTEM measurements are prepared via dropcasting a droplet of ethanol suspension onto a copper grid, coated with a thin layer of amorphous carbon film, and allowed to dry in air. Note that the hierarchical Zn_2GeO_4 core-shell microspheres are firstly sonicated for 1 h to obtain dispersive fragments and then used for TEM and HRTEM measurement. The X-ray diffraction patterns (XRD) of the products are recorded with Bruker D8 Focus Diffraction System using a Cu Kα source (λ = 0.154178 nm). Fourier transform infrared (FTIR) spectroscopy is recorded on a MAGNA-IR 750 (Nicolet Instrument Co.) FTIR spectrometer. The surface area and pore size distributions are determined by nitrogen physisorption using Quadrasorb SII Quantachrome Instrument. The surface area is calculated using the Brunauer-Emmett-Teller (BET) method. Pore size distributions are calculated using the Barrett-Joyner-Halenda (BJH) method from the desorption branch. Photoluminescence (PL) emission spectra generated luminescent 2-hydroxyterephthalic acid (TAOH) is measured on a Hitachi F-2500 fluorescence spectrophotometer. The UV-Vis absorption spectra were recorded on a UV-Vis spectrophotometer (TU-1901).

2.4 Photocatalytic activity

Photocatalytic activities of hierarchical Zn_2GeO_4 core-shell microspheres compounds are evaluated by the degradation of methyl orange (MO) and phenol in water under UV irradiation from a 200 W UV light lamp. For the degradation of MO, 0.1 g of the Zn_2GeO_4 samples is dispersed in 150 mL of an aqueous solution of MO (15 mg L^{-1}). Prior to UV light illumination, the solution is continuously stirred for 30 min in the dark to ensure the establishment of an adsorption-desorption equilibrium between the photocatalysts and the dye. After that, the solution is exposed to UV irradiation under magnetic stirring. At given time intervals, 5 mL of the suspension is taken out and centrifuged to remove the photocatalyst. Then, the filtrates are analyzed by recording variations of the absorption band maximum (464 nm) in the UV-visible spectra of the dye MO. For the photocatalytic degradation of phenol, the initial concentration of the phenol solution is 10 mg/L and other conditions are kepted unchanged. After UV-light irradiation for a special time interval, the filtrates are analyzed by recording variations of the absorption band maximum (271 nm) of phenol.

2.5 Detection of reactive species

Measurements of hydroxyl radicals ($^{\cdot}$OH) on the surface of UV-illuminated hierarchical Zn_2GeO_4 core-shell microspheres are carried out by the terephthalic acid (TA) fluorescence probe method. 0.1 g of hierarchical Zn_2GeO_4 core-shell microspheres is dispersed in a 150 mL of 5×10^{-4} M terephthalic acid aqueous solution with a concentration of 2×10^{-3} M NaOH. The experiment is carried out under UV irradiation using a 200 W UV light lamp. After UV irradiation at a time interval of 5 min, the reaction solution is filtrated to measure the increase in the PL intensity at 426 nm of TAOH excited by 312 nm light.

3. Results and discussion

3.1 Characterization of hierarchical Zn_2GeO_4 core-shell microspheres

The hierarchical Zn_2GeO_4 core-shell microspheres are synthesized through a facile hydrothermal method. GeO_2 and ZnO are added into the mixture of deionized water and triethylenetetramine (TETA) at 220 ^{o}C for 24 h. The as-prepared products are firstly characterized by scanning electron microscopy (SEM), transmission electron microscopy (TEM) and X-ray diffraction (XRD). Low-magnified SEM images (Fig. 1a and Fig. S1†) show that Zn_2GeO_4 microspheres are successfully fabricated in large quantities and with a size distribution about 5-6 μm. The typical XRD pattern displayed in Fig. 1i identifies these microspheres as a highly crystalline rhombohedral phase of Zn_2GeO_4 (JCPDS No. 11-0687) with a space group of R-3(148)

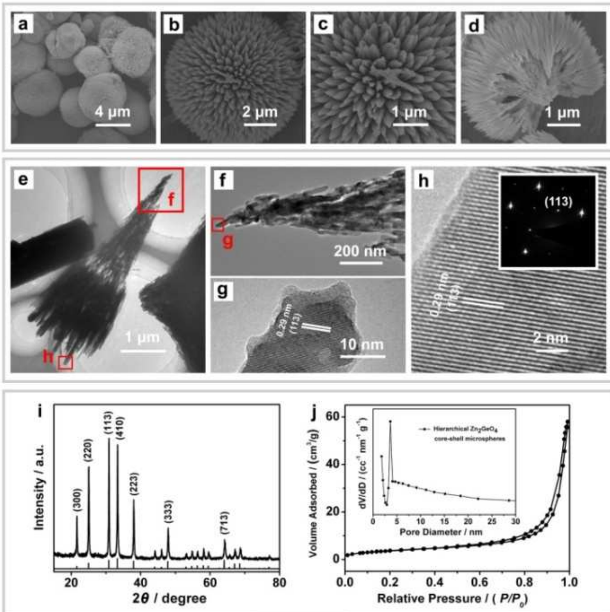

Fig. 1 SEM images (a-d) of the hierarchical Zn_2GeO_4 core-shell microspheres synthesized through a facile hydrothermal method. (e) TEM image of the partial components of Zn_2GeO_4 building block. (f) TEM image of the stacked nanoparticles at the core of the hierarchical Zn_2GeO_4 core-shell microspheres. (g) HRTEM image of the nanopartice at the core of the hierarchical Zn_2GeO_4 core-shell microspheres. (h) HRTEM image and SAED pattern of the rod at the shell of the hierarchical Zn_2GeO_4 core-shell microspheres. (i) XRD pattern and (j) N_2 adsorption/desorption isotherm and Barrett-Joyner-Halenda (BJH) pore size distribution plot (inset) of the hierarchical Zn_2GeO_4 core-shell microspheres.

and lattice constants of $a = b = 1.423$ nm, $c = 0.953$ nm, $\alpha = \beta = 90°$, and $\gamma = 120°$. No any additional peak is observed, indicating high purity of the resulting Zn_2GeO_4 samples. Energy-dispersive spectroscopy (EDS) analysis (Fig. S2†) and Fourier-transform infrared spectroscopy (FTIR) (Fig. S3†) further support the results mentioned above. High-magnification SEM images (Fig. 1b and 1c) reveal that the individual microsphere is composed of 1D Zn_2GeO_4 rod-shaped nanostructure, indicating its nature of hierarchical structure. The cracked microspheres (Fig. 1d and S4†) show that the as-obtained Zn_2GeO_4 microsphere consists of two parts, interior core and external shell. The interior region is mainly composed of stacked nanoparticles, while, the external shell is built from orderly paralled and overlapped rod-like microcrystals with a diameter of 50-100 nm and length of 1-2 μm. The results demonstrate that the as-prepared Zn_2GeO_4 microspheres possess a typical hierarchical core-shell structure. To further confirm the proposed structure, a sonication treatment is made to obtain partial components of Zn_2GeO_4 building block for TEM characterization. As shown in Fig. 1e, the TEM image clearly demonstrates the hierarchical core-shell nature of these Zn_2GeO_4 microspheres. The core is stacked with single-crystalline nanoparticles (Fig. 1f and 1g) and the shell contains well-aligned rods (Fig. 1f). HRTEM image (Fig. 1h) displays that the rods own an interplanar distance of 0.29 nm, corresponding to the (113) *d*-spacing of the rhombohedral Zn_2GeO_4 structure.[50, 59] The corresponding selected area electron diffraction (SAED) pattern (the inset of Fig. 1h) reveals apparent single-crystalline characteristics of the as-prepared Zn_2GeO_4 nanorods. Fig. 1j shows the N_2 adsorption/desorption isotherm and Barrett-Joyner-Halenda (BJH) pore size distribution plot of hierarchical Zn_2GeO_4 core-shell microspheres. The shape of the isotherm seems to nearly be a type IV isotherm according to the IUPAC classification, indicating the presence of mesopores.[60] The pore size is about 3.7 nm according to the Barrett-Joyner-Halenda pore size distribution obtained from the isotherm. The wide distribution of pore size is due to the void between the aggregated nanorods. The surface area of the hierarchical Zn_2GeO_4 core-shell microspheres determined by BET method is 13.7 m^2 g^{-1}. These results clearly illuminate that the hierarchical Zn_2GeO_4 core-shell microspheres with mesopores can be obtained through a mild hydrothermal route.

3.2 Formation mechanism of the hierarchical Zn_2GeO_4 core-shell microspheres

To shed light on the formation mechanism of the hierarchical Zn_2GeO_4 core-shell microspheres, time-dependent experiments are performed. SEM and XRD are adopted to characterize the intermediates collected at different reaction stages. At the early stage for 1 h, Zn_2GeO_4 nanoparticles are dominant (Fig. 2a), indicating that the primary nucleation growing to coarsening particles takes place in a very short time. The associated XRD pattern (Fig. S5†) shows that the intermediates collected at 1 h have already been Zn_2GeO_4 phase. The result is mainly attributed to that TETA molecules, as a strong chelating agent in alkaline solution, can coordinate with Zn^{2+} to form a Zn(II)-TETA complex, and GeO_2 is dissolved in alkaline solution to give GeO_3^{2-} ions. Then the Zn(II)-TETA complex reacts with the

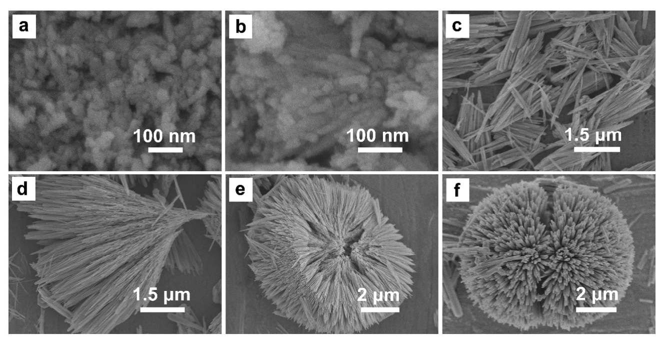

Fig. 2 SEM images of the representative intermediates collected after the reaction proceeds for 1 h (a); 2 h (b); 6 h (c); 10 h (d); 12 h (e) and 18 h (f), respectively.

GeO_3^{2-} ion to obtain Zn_2GeO_4 colloids.[61] Under high pressure and temperature conditions, tiny Zn_2GeO_4 nanoparticles are produced in the supersaturated solution.[62] When the reaction time increases to 2 h, orderly linked and elongated nanoparticle-array appears (Fig. 2b). Following at 6 h, the dispersive elongated rod-like structure with diameter about 50 nm and length up to 3-5 μm is observed, thus demonstrating that primary nanoparticles can act as building blocks for the formation of Zn_2GeO_4 nanorods (Fig. 2c). The results are in correspondence with the previous reports.[53, 55, 57, 63] In the mixed solution of alkylamine and H_2O, alkylamine molecules perform a multifunctional role as a structure-director and regulator in selectively adsorbing and binding on specific panels to control the direction of crystal growth for one-dimensional structures; simultaneously, the presence of H_2O assists to partially protonate alklyamine molecules, and further moderates the coordination and H-bonding interaction between alkylamines and Zn_2GeO_4. In our system, TETA molecules can selectively bind to some specific panels, resulting a preferential crystal growth, which is termed as the solvent-coordination molecular-template (SCMT).[53, 57, 63] Elongation of the reaction to 10 h generates fan-like structures with radiating fantails *via* the self-assembly of partial nanorods (Fig. 2d). In the pure TETA solvent, only bulk Zn_2GeO_4 structures are generated (Fig. S6†); while, in the absence of TETA molecules, only prismatic rod-like structure is obtained (Fig. S7†), demonstrating the synergistic effect of TETA and H_2O molecules is vital for the assembly process of the fan-like structures. The preferential attachment of TETA molecules to specific surfaces results in strongly mutual interactions between the rods by van der Waals forces. Additionally, small lateral adhesion energy facilitates them to attach together. Since the rod-like crystallites located in the inner region of the fan-like assembly have higher surface energy than that of the external part, they easily dissolved compared to those on the outside.[56] In the subsequent ripening and crystallization process, the inner parts of the fan-like assembly become fluffy particle-stacked structure due to the dissolution for surface energy minimization. Although the surface-to-surface conjunctions take place between the nanorods, the width and length of the rods don't take any change, implying that thermodynamic equilibrium of growth has been already reached before the assembly behaviour occurs. We speculate the ensembled fan-like structure as a monomer. Under the driving force of TETA molecules, in the next stage at 12 h, the monomer-by-monomer secondly self-assembles into hemisphere (Fig. 2e). As the reaction proceeds to 18 h, the hemisphere sequentially attaches onto another hemisphere with a match to their specific crystallographic orientation (Fig. 2f). Thus, it can be speculated that as-formed hemispheres have a predominant tendency to further aggregate together into hierarchical spheres at present conditions. The phenomenon may be ascribed to the fact that the surface energy of an individual hemisphere is relatively high based on the thermodynamics, and thus tending to decrease to the substantial minimization of surface energy by aggregation into spherical structures.[64-66] This assumption is further proved to be reasonable by the final formation of the microspherical structures collected at 24 h (Fig. 1a, 1b). Meanwhile, the as-formed hierarchical Zn_2GeO_4 core-shell microspheres possess a high degree of structure integrity, which may be associated with the Ostwald ripening process.[67] Based on these above-mentioned results, the formation mechanism involves the solvent-coordination molecular-template (SCMT) process and triethylenetetramine (TETA)-induced self-assembly route under a solvothermal condition, as shown in Scheme 1.

3.3 Diverse types of hierarchical Zn_2GeO_4 structures

In addition, it is found that diverse types of hierarchical Zn_2GeO_4 structures can be obtained by simply diluting the reactant concentration, changing reaction temperature or adjusting the volume ratio of TETA:H_2O. Here, three representative hierarchical Zn_2GeO_4 morphologies are introduced. When the reactant concentration is diluted by 5 times while other conditions are kept unchanged, dumbbell-like structure composed of well-aligned nanorod building blocks is synthesized (Fig. 3a). All the detectable reflection peaks of the XRD pattern (Fig. 3b) could be

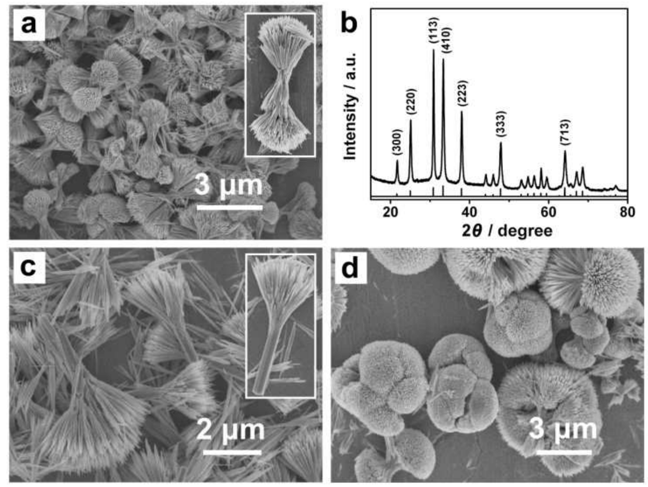

Fig. 3 Diverse types of hierarchical Zn_2GeO_4 structures synthesized at different conditions. (a) SEM image and (b) XRD pattern of the dumbbell-like Zn_2GeO_4 structure, which is fabricated by adding 0.0213 g GeO_2 and 0.0326 g ZnO into the mixed solvent of 8 mL distilled water and 5 mL TETA at 220 °C for 24 h. (c) SEM image of the broom-like Zn_2GeO_4 structure, which is obtained by adding 0.0213 g GeO_2 and 0.0326 g ZnO into the mixed solution of 8 mL distilled water and 5mL TETA at 200 °C for 24 h. (d) SEM image of the mushroom-shaped Zn_2GeO_4 strucures, which is synthesized by adding 0.0213 g GeO_2 and 0.0326 g ZnO into the mixed solution of 2 mL distilled water and 11 mL TETA at 220 °C for 24 h.

assigned to a rhombohedral phase of Zn_2GeO_4 (JCPDS No. 11-0687), thus suggesting that changing the experiment parameter only influences the hierarchical morphology but it has no effect on the crystal phase. In this hydrothermal system, a decreased reactant concentration leads to a lower supersaturation, which effectively slows the reactivity rate and diffusion behaviour of the reagents and avoids the excessive agglomeration of the building blocks under the driving force of the TETA molecules.[63, 66] In other words, various hierarchical Zn_2GeO_4 structures with aligned nanorod building blocks may be selectively fabricated by rationally tuning the supersaturation. Under the above conditions, decreasing the temperature to 200 °C results in the broom-like Zn_2GeO_4 structure (Fig. 3b). The structure is composed of a prismatic backbone and a fantail with well-aligned nanorods oriented to a center and radically sputtering out at one end. The obvious difference in this morphology is the formation of prismatic backbone, which may result from the decreased temperature. Just as stated in the previous report, an appropriate reaction temperature is favourable for the formation of relatively dispersive prismatic rods.[68, 69] When adjusting the volume ratio of TETA: H_2O from 5:8 to 11:2 at 220 °C, hierarchical mushroom-shaped Zn_2GeO_4 structures are dominant (Fig. 3d). It should be noted that the fan-like monomers, composed for the mushroom-shaped Zn_2GeO_4 structure, are not aligned well compared with that of the hierarchical Zn_2GeO_4 core-shell microspheres (Fig. 1a-c). This may be attributed to the discrepant structure-directing effect and driving force of TETA molecules in a different mixed solvents.[53, 59, 63] These extending works indicate that various hierarchical Zn_2GeO_4 structures can be selectively prepared by rationally tuning the reaction parameters. Efforts to synthesize diverse artistical morphologies and to get deeper insights in the formation mechanism are underway in our group.

3.4 Photocatalytic performance

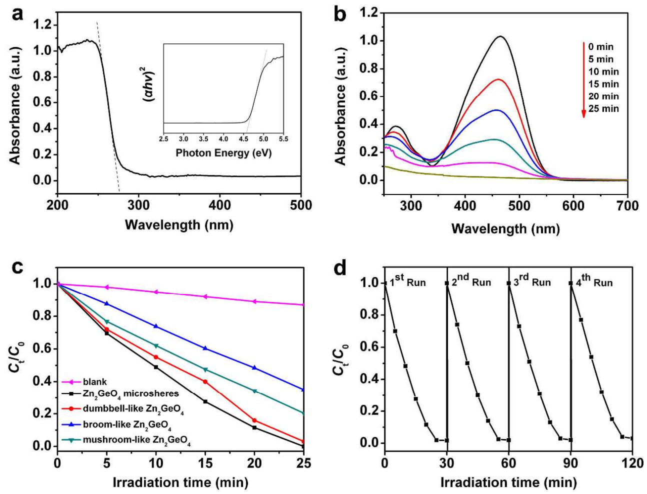

Fig. 4 (a) Diffuse reflectance spectrum (DRS) for the hierarchical Zn_2GeO_4 core-shell microspheres. The inset is the optical band gap energy *Eg* of Zn_2GeO_4 (4.56 eV). (b) Representative methyl orange (MO) dye degradation temporal profile. (c) Rate of photocatalytic degradation of methyl orange over different Zn_2GeO_4 structures as a function of reaction time. (d) Catalyst cycling in the photocatalytic degradation of methyl orange in the presence of hierarchical Zn_2GeO_4 core-shell microspheres under UV irradiation. The initial concentration and volume of MO aqueous solution is maintained at 15 mg/L and 150 mL, respectively, in each run.

As shown in Fig. 4a, the spectrum absorption edge of Zn_2GeO_4 microspheres is located at 275 nm, and the band gap is estimated as 4.56 eV, based on $\alpha h\nu = A(h\nu - Eg)^{n/2}$, in which α, ν, A, and Eg signify the absorption coefficient, light frequency, proportionality constant, and band gap, respectively. Here n is equal to 1 as the material is a direct-gap semiconductor.[70-72] The photocatalytic activity of the as-obtained hierarchical Zn_2GeO_4 core-shell microspheres are evaluated by the photocatalytic degradation of dye methyl orange (MO) in aqueous solution. To conduct the photocatalytic degradation experiment, 0.1 g of the Zn_2GeO_4 sample is dispersed in 150 mL of an aqueous solution of MO (15 mg L^{-1}). Prior to UV light illumination, the solution is continuously stirred for 30 min in the dark to ensure the establishment of an adsorption-desorption equilibrium. And the adsorption of MO is negligible. The irradiation is performed with a 200 W UV light lamp. At given time intervals, about 5 mL of the suspension is taken out and centrifuged to remove the photocatalysts. Then, the filtrates are analyzed by recording variations of the absorption band maximum (464 nm) in the UV-Visible spectra of the dye MO by using a UV-Vis spectrophotometer. Fig. 4b shows the representative MO dye degradation temporal profile over the hierarchical Zn_2GeO_4 core-shell microspheres under UV-light irradiation. The intensity of the absorption peak at 464 nm decreases gradually with increasing UV exposure time and almost disappears after 25 min, which means that the nitrogen to nitrogen double bond of MO is destroyed. Fig. 4c presents the concentration changes of MO as a function of irradiation time during the degradation process. After UV-light irradiation for 25 min, the degradation of MO on hierarchical Zn_2GeO_4 core-shell microspheres reaches 100%, exceeding the degradation of MO on dumbbell-like Zn_2GeO_4 structures (Fig. 3a), broom-like Zn_2GeO_4 structures (Fig. 3c), mushroom-shaped Zn_2GeO_4 structures (Fig. 3d) and self-photolysis rate of MO. The higher photocatalytic activity of the hierarchical Zn_2GeO_4 core-shell microspheres may be attributed to the unique hierarchical core-shell structures, large specific surface area, rich reaction sites and more efficient transfer of the photogenerated charges.[73, 74] The durability of the hierarchical Zn_2GeO_4 core-shell microspheres is also evaluated by reusing the catalyst for four runs towards the decomposition of MO under the same condition. As shown in Fig. 4d, the catalyst almost affords the same photocatalytic activity as the initial one, demonstrating its excellent photocatalytic stability. SEM images (Fig. S8†) and XRD pattern (Fig. S9†) of the recycled catalysts reveal that these hierarchical Zn_2GeO_4 core-shell microspheres do not experience any obvious change during the photocatalytic process, and thus suggesting their good stability of morphology and phase structure. These results display that hierarchical Zn_2GeO_4 core-shell microspheres are effective and stable catalysts for the decomposition of MO in aqueous solution.

In addition to the decoloration of MO, phenol is utilized to further evaluate the photocatalytic activities of the hierarchical Zn_2GeO_4 core-shell microspheres. Under UV irradiation, the absorption peak of phenol solution at 271 nm decreases with the increased irradiation time in the presence of Zn_2GeO_4 (Fig. S10†), while the decrease of the absorption peak of self-degradated phenol solution is inconspicuous in the control experiment, and thus indicating that the as-prepared hierarchical Zn_2GeO_4 core-shell microspheres possess efficient UV photocatalytic activity towards photocatalytic degradation of phenol. Simultaneously, it can prove that the decomposition of MO is catalyzed by the hierarchical Zn_2GeO_4 core-shell microsphere catalysts but not caused by the photosensitization process.[75]

3.5 Photocatalytic mechanism

To detect the active species involved in the photocatalytic process, the terephthalic acid (TA) fluorescence probe method is used to detect $\cdot OH$ radicals.[73, 76] After UV irradiation at a time interval of 5 min, the terephthalic acid (TA) solution is filtrated to measure the photoluminescence (PL) emission spectra excited at 312 nm. As shown in Fig. 5a, it can be seen that the intensity of the PL emission spectra at 426 nm increases with the extended reaction time, demonstrating that the $\cdot OH$ radicals are the active species in the photocatalytic process.

To get insight into the underlying mechanism of photocatalytic degradation of MO over hierarchical Zn_2GeO_4 core-shell microspheres, a series of control experiments are performed. As shown in Fig. 5b, different radical quenchers are employed to tscavenge the counterpart active species, such as, isopropanol (IPA, 2.0 mM) as scavenger for hydroxyl radical ($\cdot OH$), benzoquinone (BQ, 2.0 mM) as scavenger for superoxide radical ($\cdot O_2^-$), and ammonium oxalate (AO, 2.0 mM) as scavenger for photogenerated holes (h^+), respectively.[77, 78] The addition of IPA and BQ results in an obvious degradation efficiency of MO catalyzed by the hierarchical Zn_2GeO_4 core-shell microspheres, proving that $\cdot OH$ and $\cdot O_2^-$ are the main active species in the photodegradation process. While the presence of AO has a relatively small influence on the decomposition of MO, and thus indicating that h^+ is not the predominant active species in the photocatalytic process, which may be attributed to its rapid consumption by oxidation of H_2O or OH^- to $\cdot OH$.

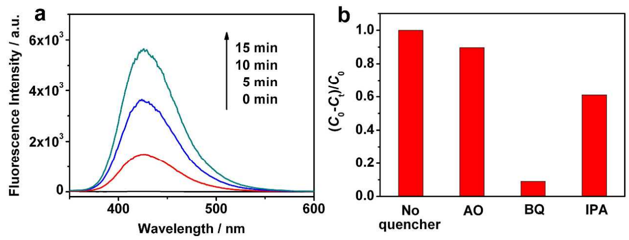

Fig. 5 (a) Time-dependent fluorescence emission spectra of TAOH formed by the reaction of TA with ·OH radicals; (b) Trapping experiments of active species during the photocatalytic reaction by the hierarchical Zn_2GeO_4 core-shell microspheres photocatalyst towards degradation of MO under UV-light irradiation.

Based on the above-mentioned results, a possible mechanism for the photocatalytic degradation of dyes or organic pollutants by the hierarchical Zn_2GeO_4 core-shell microspheres is proposed (Scheme 2). Under UV-light irradiation ($h\nu > Eg = 4.68$ eV), Zn_2GeO_4 catalyst is activated to generate long-lived electron-hole pairs, including conduction band electrons (e^-) and valence band holes (h^+). Then, the reductive photo-generated electron (e^-) is scavenged by O_2 to produce superoxide radical anions ($^{\cdot}O_2^-$), which posseses strong oxidative capability of decomposing MO and phenol in aqueous solution. The oxidative photo-generated holes (h^+) can react with surface adsorbed H_2O or OH^- to yield ·OH radicals, which exert a noticeable positive influence on oxidizing the organic molecule to form small molecule products.

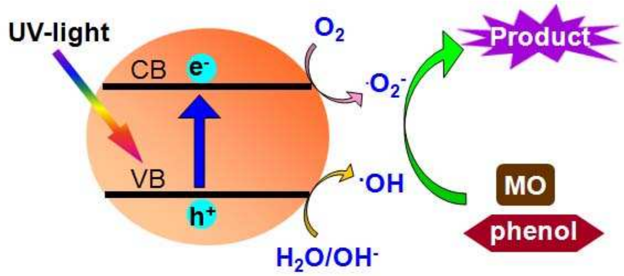

Scheme 2. Schematic illustration of the photocatalytic mechanism of organic pollutants degradation over hierarchical Zn_2GeO_4 core-shell microspheres catalyst.

4. Conclusions

In summary, hierarchical Zn_2GeO_4 core-shell microspheres composed of stacked nanoparticles at the core and well-aligned rods at the shell are prepared via a mild hydrothermal hard-template-free method. The formation mechanism involves the solvent-coordination molecular-template (SCMT) process and triethylenetetramine (TETA)-induced self-assembly route. The as-obtained hierarchical Zn_2GeO_4 core-shell microspheres exhibit excellent photocatalytic activity and stability toward dyes degradation. In addition, other hierarchical Zn_2GeO_4 structures with diverse types of morphologies can be selectively prepared by rationally tuning the reaction conditions. The present synthetic strategy may allow access to fabricating other multifunctional materials with special artistical morphologies.

Acknowledgement

This work was financially supported by the National Natural Science Foundation of China (No. 21422104 and No. 21373149) and the Innovation Foundation of Tianjin University.

Notes and references

[a] *Department of Chemistry, School of Science, Tianjin University Collaborative Innovation Center of Chemical Science and Engineering Tianjin, 300072, China; E-mail: bzhang@tju.edu.cn*

† Electronic Supplementary Information (ESI) available: Experimental details, characterization, Fig. S1-S9†, their captions, and supplementary discussions. See DOI: 10.1039/b000000x/

1. J. Du, X. Lai, N. Yang, J. Zhai, D. Kisailus, F. Su, D. Wang and L. Jiang, *ACS Nano*, 2011, **5**, 590-596.
2. J. Xiong, Z. Jiao, G. Lu, W. Ren, J. Ye and Y. Bi, *Chem. Eur. J.*, 2013, **19**, 9472-9475.
3. Z. Haider and Y. S. Kang, *ACS Appl. Mater. Interfaces*, 2014, **6**, 10342-10352.
4. J. Shi, Y. Liu, Q. Peng and Y. Li, *Nano Res*, 2013, **6**, 441-448.
5. D. K. Roh, W. S. Chi, H. Jeon, S. J. Kim and J. H. Kim, *Adv. Funct. Mater.*, 2014, **24**, 379-386.
6. J. S. Chen, Y. L. Tan, C. M. Li, Y. L. Cheah, D. Luan, S. Madhavi, F. Y. C. Boey, L. A. Archer and X. W. Lou, *J. Am. Chem. Soc.*, 2010, **132**, 6124-6130.
7. D. D. Vaughn II, O. D. Hentz, S. Chen, D. Wang and R. E. Schaak, *Chem. Commun.*, 2012, **48**, 5608-5610.
8. C. Sun, S. Rajasekhara, J. B. Goodenough and F. Zhou, *J. Am. Chem. Soc.*, 2011, **133**, 2132-2135.
9. L. D. Zhao, V. P. Dravid and M. G. Kanatzidis, *Energy Environ. Sci.*, 2014, **7**, 251-268.
10. L.-D. Zhao, S. Hao, S.-H. Lo, C.-I. Wu, X. Zhou, Y. Lee, H. Li, K. Biswas, T. P. Hogan, C. Uher, C. Wolverton, V. P. Dravid and M. G. Kanatzidis, *J. Am. Chem. Soc.*, 2013, **135**, 7364-7370.
11. H.-B. Yao, H.-Y. Fang, X.-H. Wang and S.-H. Yu, *Chem. Soc. Rev.*, 2011, **40**, 3764-3785.
12. G. Tian, Y. Chen, W. Zhou, K. Pan, C. Tian, X.-r. Huang and H. Fu, *CrystEngComm*, 2011, **13**, 2994-3000.
13. J. Xiong, Q. Dong, T. Wang, Z. Jiao, G. Lu and Y. Bi, *RSC Adv.*, 2014, **4**, 583-586.
14. M. Raula, M. H. Rashid, T. K. Paira, E. Dinda and T. K. Mandal, *Langmuir*, 2010, **26**, 8769-8782.
15. F. J. Douglas, D. A. MacLaren, F. Tuna, W. M. Holmes, C. C. Berry and M. Murrie, *Nanoscale*, 2014, **6**, 172-176.
16. L. Li, K. H. Seng, Z. Chen, Z. Guo and H. K. Liu, *Nanoscale*, 2013, **5**, 1922-1928.
17. K. Miszta, J. de Graaf, G. Bertoni, D. Dorfs, R. Brescia, S. Marras, L. Ceseracciu, R. Cingolani, R. van Roij, M. Dijkstra and L. Manna, *Nat. Mater.*, 2011, **10**, 872-876.
18. Z. Zhang, Y. Chen, S. He, J. Zhang, X. Xu, Y. Yang, F. Nosheen, F. Saleem, W. He and X. Wang, *Angew. Chem. Int. Ed.*, 2014, **53**, 1-6.
19. R. H. Coridan, K. A. Arpin, B. S. Brunschwig, P. V. Braun and N. S. Lewis, *Nano Lett.*, 2014, **14**, 2310-2317.
20. L. Mazeina, Y. N. Picard and S. M. Prokes, *Cryst. Growth Des.*, 2009, **9**, 1164-1169.
21. L. Mazeina, Y. N. Picard, S. I. Maximenko, F. K. Perkins, E. R. Glaser, M. E. Twigg, J. A. Freitas, Jr. and S. M. Prokes, *Cryst. Growth Des.*, 2009, **9**, 4471-4479.
22. J. Zhu, Z. Yin, D. Yang, T. Sun, H. Yu, H. E. Hoster, H. H. Hng, H. Zhang and Q. Yan, *Energy Environ. Sci.*, 2013, **6**, 987-993.
23. Y. Zhang, Y. Tang, S. Yin, Z. Zeng, H. Zhang, C. M. Li, Z. Dong, Z. Chen and X. Chen, *Nanoscale*, 2011, **3**, 4074-4077.
24. G. Tian, Y. Chen, W. Zhou, K. Pan, Y. Dong, C. Tian and H. Fu, *J. Mater. Chem.*, 2011, **21**, 887-892.
25. J. G. Yu, J. C. Yu, L. Z. Zhang, X. C. Wang and L. Wu, *Chem. Commun.*, 2004, 2414-2415.
26. X. J. Li, W. Xing, J. Zhou, G. Q. Wang, S. P. Zhuo, Z. F. Yan, Q. Z. Xue and S. Z. Qiao, *Chem. Eur. J.*, 2014, **20**, 1-8.
27. P. R. Sajanlal and T. Pradeep, *Nano Res*, 2009, **2**, 306-320.
28. M. Pradhan, J. Chowdhury, S. Sarkar, A. K. Sinha and T. Pal, *J. Phys. Chem. C*, 2012, **116**, 24301-24313.
29. J. Liang, X. Du, C. Gibson, X. W. Du and S. Z. Qiao, *Adv. Mater.*, 2013, **25**, 6226-6231.

30. M. Rose, Y. Korenblit, E. Kockrick, L. Borchardt, M. Oschatz, S. Kaskel and G. Yushin, *Small*, 2011, **7**, 1108-1117.
31. W. Ho, J. C. Yu and S. Lee, *Chem. Commun.*, 2006, 1115-1117.
32. L. Li, R. Cao, Z. Wang, J. Li and L. Qi, *J. Phys. Chem. C*, 2009, **113**, 18075-18081.
33. M. Muruganandham and Y. Kusumoto, *J. Phys. Chem. C*, 2009, **113**, 16144-16150.
34. Y. N. Ko, S. H. Choi, S. B. Park and Y. C. Kang, *Nanoscale*, 2014, **6**, 10511-10515.
35. L. Su, Y. Zhong and Z. Zhou, *J. Mater. Chem. A*, 2013, **1**, 15158-15166.
36. X. Li, M. Li, P. Cui, X. Zhao, T. Gu, H. Yu, Y. Jiang and D. Song, *CrystEngComm*, 2014, **16**, 3834-3838.
37. F. Li, M. Morris and K.-Y. Chan, *J. Mater. Chem.*, 2011, **21**, 8880-8886.
38. Q. Liu, Y. Zhou, W. Tu, S. Yan and Z. Zou, *Inorg. Chem.*, 2014, **53**, 359-364.
39. S. A. S. de Farias, M. V. Lalic and J. B. L. Martins, *Chem. Phys. Lett.*, 2013, **578**, 76-80.
40. F. Zou, X. Hu, Y. Sun, W. Luo, F. Xia, L. Qie, Y. Jiang and Y. Huang, *Chem. Eur. J.*, 2013, **19**, 6027-6033.
41. S. Wu, R. Wang, Z. Wang and Z. Lin, *Nanoscale*, 2014, **6**, 8350-8358.
42. S. Takeshita, J. Honda, T. Isobe, T. Sawayama and S. Niikura, *Cryst. Growth Des.*, 2010, **10**, 4494-4500.
43. S.-P. Liu, M.-L. Chen, B.-C. Chang and K.-H. Lii, *Inorg. Chem.*, 2013, **52**, 3990-3994.
44. J. Wang, C. Yan, S. Magdassi and P. S. Lee, *ACS Appl. Mater. Interfaces*, 2013, **5**, 6793-6796.
45. L. Sun, Y. Qi, C.-J. Jia, Z. Jin and W. Fan, *Nanoscale*, 2014, **6**, 2649-2659.
46. J. Liu, G. K. Zhang, J. C. Yu and Y. D. Guo, *Dalton trans.*, 2013, **42**, 5092-5099.
47. B. Ma, F. Wen, H. Jiang, J. Yang, P. Ying and C. Li, *Catal. Lett.*, 2010, **134**, 78-86.
48. N. Zhang, S. Ouyang, P. Li, Y. Zhang, G. Xi, T. Kako and J. Ye, *Chem. Commun.*, 2011, **47**, 2041-2043.
49. M.-Y. Tsai, C.-Y. Yu, C.-C. Wang and T.-P. Perng, *Cryst. Growth Des.*, 2008, **8**, 2264-2269.
50. J. Huang, X. Wang, Y. Hou, X. Chen, L. Wu and X. Fu, *Environ. Sci. Technol.*, 2008, **42**, 7387-7391.
51. H. W. Kim, H. G. Na, J. C. Yang and C. Lee, *Chem. Eng. J.*, 2011, **171**, 1439-1445.
52. C. Y. Yan and P. S. Lee, *J. Phys. Chem. C*, 2009, **113**, 14135-14139.
53. Q. Liu, Y. Zhou, J. Kou, X. Chen, Z. Tian, J. Gao, S. Yan and Z. Zou, *J. Am. Chem. Soc.*, 2010, **132**, 14385-14387.
54. L. Yu, R. Zou, Z. Zhang, G. Song, Z. Chen, J. Yang and J. Hu, *Chem. Commun.*, 2011, **47**, 10719-10721.
55. T. Wang, Q. Liu, G. Li, K. B. Xu, R. J. Zou and J. Q. Hu, *CrystEngComm*, 2014, **16**, 3222-3227.
56. J. Liang, J. Xu, J. Long, Z. Zhang and X. Wang, *J. Mater. Chem. A*, 2013, **1**, 10622-10625.
57. J. Liang, J. Xu, Q. Gu, Y. Zhou, C. Huang, H. Lina and X. Wang, *J. Mater. Chem. A*, 2013, **1**, 7798-7805.
58. C. W. Sun, S. Rajasekhara, Y. J. Chen and J. B. Goodenough, *Chem. Commun.*, 2011, **47**, 12852-12854.
59. Y. Sun, L. Yu and P. Rao, *J. Cryst. Growth*, 2012, **347**, 73-76.
60. C. Yuan, X. Zhang, L. Su, B. Gao and L. Shen, *J. Mater. Chem.*, 2009, **19**, 5772-5777.
61. L. Zhang, X.-F. Cao, Y.-L. Ma, X.-T. Chen and Z.-L. Xue, *CrystEngComm*, 2010, **12**, 3201-3206.
62. D. Gebauer, M. Kellermeier, J. D. Gale, L. Bergstrom and H. Cöelfen, *Chem. Soc. Rev.*, 2014, **43**, 2348-2371.
63. Q. Liu, Y. Zhou, Z. Tian, X. Chen, J. Gao and Z. Zou, *J. Mater. Chem.*, 2012, **22**, 2033-2038.
64. L. Hu, H. Zhong, X. Zheng, Y. Huang, P. Zhang and Q. Chen, *Sci. Rep.*, 2012, **2**, 1-8.
65. H. Colfen and S. Mann, *Angew. Chem. Int. Ed.*, 2003, **42**, 2350-2365.
66. H. Cölfen and M. Antonietti, *Angew. Chem. Int. Ed.*, 2005, **44**, 5576-5591.
67. F. Dong, W.-K. Ho, S. C. Lee, Z. Wu, M. Fu, S. Zou and Y. Huang, *J. Mater. Chem.*, 2011, **21**, 12428-12436.
68. L. Zhang, L. Lian, J.-S. Dai and Y. Liu, *Micro Nano Lett.*, 2012, **7**, 1143-1146.
69. S. C. Yan, L. J. Wan, Z. S. Li and Z. G. Zou, *Chem. Commun.*, 2011, **47**, 5632-5634.
70. S. Ilican, Y. Caglar, M. Caglar and F. Yakuphanoglu, *J. Alloy Compd.*, 2009, **480**, 234-237.
71. F. Yakuphanoglu, *J. Alloy Compd.*, 2009, **470**, 55-59.
72. K.-S. Ahn, S. Shet, T. Deutsch, C.-S. Jiang, Y. Yan, M. Al-Jassim and J. Turner, *J. Power Sour.*, 2008, **176**, 387-392.
73. J. Liu and G. Zhang, *CrystEngComm*, 2013, **15**, 382-389.
74. L. P. Zhu, N. C. Bing, L. L. Wang, H. Y. Jin, G. H. Liao and L. J. Wang, *Dalton trans.*, 2012, **41**, 2959-2965.
75. W. Wang, H. Cheng, B. Huang, X. Li, X. Qin, X. Zhang and Y. Dai, *Inorg. Chem.*, 2014, **53**, 4989-4993.
76. Z. Wan, G. Zhang, J. Wang and Y. Zhang, *RSC Adv.*, 2013, **3**, 19617-19623.
77. W. Zhao, C. Liu, L. Cao, X. Yin, H. Xu and B. Zhang, *RSC Adv.*, 2013, **3**, 22944-22948.
78. D. Hou, X. Hu, Y. Wen, B. Shan, P. Hu, X. Xiong, Y. Qiao and Y. Huang, *Phys. Chem. Chem. Phys.*, 2013, **15**, 20698-20705.

Table of contents entry

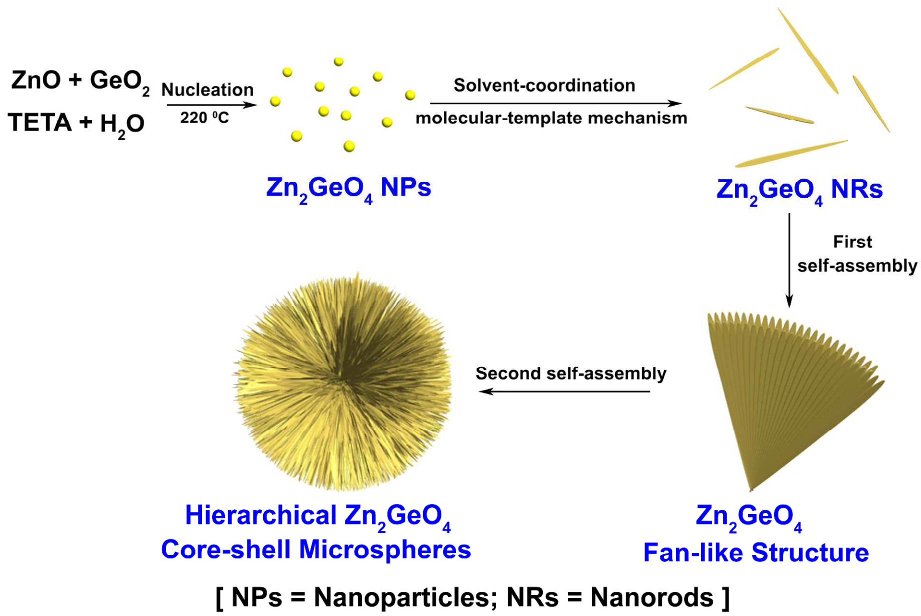

Hierarchical Zn_2GeO_4 core-shell microspheres exhibit enhanced photocatalytic activity and stability towards photocatalytic degradation of organic pollutants.